Journal of Magnetism and Magnetic Materials 395 (2015) 303–311

Contents lists available at ScienceDirect

Journal of Magnetism and Magnetic Materials

journal homepage: www.elsevier.com/locate/jmmm

Crystal structure, magnetic and dielectric behavior of h-$LuMn_xO_{3\pm\delta}$ ceramics ($0.95 \leq x \leq 1.04$)

A. Baghizadeh [a,*], J.M Vieira [a], J.S. Amaral [b], M.P. Graça [c], M.R. Soares [d], D.A. Mota [e], V.S. Amaral [b]

[a] Department of Materials & Ceramic Engineering & CICECO, Aveiro University, 3810-193 Aveiro, Portugal
[b] Physics Department & CICECO, Aveiro University, Aveiro, Portugal
[c] Department of Physics and I3N, Universidade de Aveiro, 3810-193 Aveiro, Portugal
[d] LCA- Central Analytical Laboratory & CICECO, Aveiro University, Aveiro, Portugal
[e] IFIMUP and IN-Institute of Nanoscience and Nanotechnology, Departamento de Física e Astronomia da Faculdade de Ciências, Universidade do Porto, Rua do Campo Alegre, 687, 4169-007 Porto, Portugal

ARTICLE INFO

Article history:
Received 26 March 2015
Received in revised form
4 July 2015
Accepted 25 July 2015
Available online 30 July 2015

Keywords:
Multiferroic
Hexagonal $LuMnO_3$
Vacancy
Magnetoelectric coupling

ABSTRACT

Lattice constants, magnetic properties and dielectric behavior of h-$LuMn_xO_{3\pm\delta}$ solid solution ($0.95 \leq x \leq 1.04$) of bulk ceramic samples prepared by the solid state reaction method were studied to determine the role of stoichiometry changes on the crystalline structure and magneto-electric coupling. It is found that increasing of Mn content results in reduction of cell volume of h-$LuMn_xO_{3\pm\delta}$ ceramics mostly due to shrinkage of a-axis length. The antiferromagnetic interactions of Mn^{3+} ions weaken with cell volume contraction. A weak ferromagnetic contribution appeared in all samples and extends up to the Neel temperature, T_N. Irreversibility in temperature dependent magnetic measurements already reported for stoichiometric compositions of hexagonal $RMnO_3$ oxides appears for all h-$LuMn_xO_{3\pm\delta}$ samples right below Neel ordering transition. An increase of magnetic coercive field and magnetization on cooling below T_N in samples is observed in field dependent magnetization and rises as x increases. In addition to the antiferromagnetic ordering transition at T_N, two anomalies of the temperature dependent magnetic susceptibility and dielectric constant are identified below T_N, centered at 69 K and 31 K respectively, being probably due to inhomogeneity of the crystalline structure inside ceramic grains. Changes of the dielectric constant at T_N can be attributed to magneto-electric coupling in the off-stoichiometric hexagonal $LuMn_xO_{3\pm\delta}$ lattice. The behavior of the dielectric relaxation follows a thermally activated mechanism with activation energy values characteristic of polaron hoping.

1. Introduction

Multiferroic hexagonal $RMnO_{3\pm\delta}$ (R=Ho-Lu, Y, Sc) materials have been investigated because they show both magnetoelectric coupling and magneto-elastic coupling, presenting open challenges to the understanding of underlying physics behind coupling of ferroic properties [1–4]. In the effort to explain and ascertain the interdependence of each ferroic property on the observed physical and chemical properties of these materials, authors have mainly dealt with A-site or B-site doping approaches [2,5–8] or by changing synthesis conditions [9–13]. Although, upon doping or changing synthesis conditions, one is able to change the ferroic properties, still from all these experimental adjustments and theoretical approaches the role of rare-earth and metal ions on unit cell parameters and magnetic and dielectric properties could not be clearly and explicitly figured out. It was found in perovskite materials like $LaMnO_{3\pm\delta}$ that creating off-stoichiometric A-site or B-site compositions would be a suitable tool for exploring the role of rare-earth (A-site) and transition metal ions (B-site) and of their effect upon the change in properties [13–18]. However, such concept has been seldom used to set the role of R and Mn ions in hexagonal rare-earth manganites [19–22]. Since Lu does not have localized $4f^{14}$ electrons, it does not carry free magnetic moment to participate in magnetic interactions in h-$LuMnO_{3\pm\delta}$ lattice and hence Mn^{3+} ions are the sole magnetic ions inside the structure. The AFM ordering is explained by the 2D magnetic interaction of frustrated Mn^{3+} ions forming trimmers of nearest neighbor Mn^{3+} ions in the triangular network of basal plane of the hexagonal lattice of the $RMnO_3$ compounds [2]. Any change in Mn or Lu will duly modify magnetic moment (interaction), dielectric polarization behavior and the magneto-electric coupling. The Lu-dependent or Mn-dependent properties may reveal additional details of

* Corresponding author.
E-mail address: ali.baghizhadeh@ua.pt (A. Baghizadeh).

http://dx.doi.org/10.1016/j.jmmm.2015.07.082
0304-8853/

the interlocked dependency of relevant properties on stoichiometry shifts set by excess of either of the Lu or Mn cations.

Based on the absence of other phases in equilibrium with the $LuMn_xO_3$ phase detectable in XRD results, the stability limits of the $LuMn_xO_{3\pm\delta}$ solid solution, x=Mn/Lu ratio, from 1100 °C to 1400 °C in air correspond to the lower and upper values of x, $x_{Low}=0.94$ and $x_{High}=1.20$ respectively [23]. Accordingly, the composition of $LuMn_xO_{3\pm\delta}$ phase in the stability range at such temperatures would accommodate Mn in excess. Based on the same criterion of analysis of XRD results the corresponding stability limits of the $YMn_xO_{3\pm\delta}$ solid solution at 1400 °C in air are $x_{Low}=0.95$ and $x_{High}=1.08$, respectively [24]. It had been reported [21] that bulk ceramic samples of $YMn_xO_{3\pm\delta}$ $(1.00\le x\le 1.15)$ prepared by the solid state reaction method are also single phase with only the hexagonal manganite phase detected in the XRD analysis. The corresponding values of Curie–Weiss temperature steadily decreased from $\theta_{CW}=-330$ K in the sample of $x=1$ to $\theta_{CW}=-542$ K for sample $YMn_{1.08}O_{3\pm\delta}$. At this composition, the value θ_{CW} clearly indicate saturation of Mn in the crystalline lattice of YMn_xO_3 while this point in the range $(1.08<x\le 1.15)$ θ_{CW} remains almost constant [21]. On the Y-rich side of $YMn_xO_{3\pm\delta}$ $(0.91\le x\le 1.00)$ bulk ceramic samples are also single phase materials within the limits of detection of the XRD technique; but the almost linear increasing of the a-axis and c-axis length from the samples of $x=1.00$ to composition $YMn_{0.95}O_{3\pm\delta}$ ceases at this point [19]. Changes of the magnetic properties of the off-stoichiometric h-$RMnO_3$ thin films have been rarely reported [22]. Metastable magnetic behavior below 42 K was reported for $YMn_{1.05}O_{3\pm\delta}$ thin film with excess of Mn [22]. Only lattice modification of the h-$RMnO_3$ (R=Y, Er and Dy) off-stoichiometric thin films were studied [12]. Stabilized by the substrate constraining, the linear increase of the out-of-plane c-axis from $ErMn_{1.39}O_{3\pm\delta}$ to $ErMn_{0.80}O_{3\pm\delta}$ composition of the thin films indicates a stability domain of the solid solution much wider than stability limits of the same hexagonal phase in polycrystalline ceramics of $ErMn_xO_{3\pm\delta}$ at 1200–1400 °C as determined by the criterion of absence of secondary phases in inspection of powder XRD results [12,24].

In this study, we have synthesized off-stoichiometric samples of $LuMn_xO_{3\pm\delta}$ within composition range $0.92\le x\le 1.12$ overlapping with solid-state solubility range to get deeper understanding upon the mutual relation of Lu and Mn ions or of the equivalent RE-site or Mn-site vacancies upon the crystalline structure and properties of the material. Effects of Mn-excess (RE-site vacancy) or Lu-excess (Mn-site vacancy) on the crystalline structure, magnetic susceptibility, magnetic field dependence of magnetization and dielectric constant of $LuMn_xO_{3\pm\delta}$ materials described in this study in general confirm relevant dependences of these properties on off-stoichiometry of sample composition. It has been noticed by first time to the knowledge of authors that the enhancement at T_N of $LuMn_xO_{3\pm\delta}$ on x displays a reversed trend to the one of $YMn_xO_{3\pm\delta}$ found in data reported in the bibliography [19,25].

2. Materials and methods

Polycrystalline $LuMn_xO_{3\pm\delta}$ samples with nominal composition in the range $(0.92\le x\le 1.12)$ were synthesized by solid state reaction from high purity oxides (99.99% purity) of Lu_2O_3 and MnO_2.

The as supplied oxides were dried, weighted in the due amounts, mixed and ground in an agate mortar. To improve homogeneity of the reacted material the high temperature process was accomplished in three steps with regrinding and pressing of the material formed as pellets by cold isostatic press at 200 MPa between each step: first reaction at 850 °C for 24 h, then at 1100 °C for 12 h and final firing at 1300 °C for 24 h, all done in air.

The lattice parameters of the $LuMn_xO_{3\pm\delta}$ solid solution and formation of secondary phases were characterized by Philips XPERT XRD Diffractometer with Cu K_α X-rays after carrying out Rietveld refinement on XRD data using Fullprof Suit package [26] .

Magnetic measurements were done with SQUID magnetometer under an applied magnetic field of 100 Oe and Vibrating Sample Magnetometer (VSM) under 500 Oe applied magnetic field in the temperature range 5–350 K. The dependence of magnetization on the magnetic field (M–H) of all samples was measured also with the SQUID magnetometer under isothermal conditions at 5 K, 80 K, 120 K and at room temperature with applied fields spanning from –5.5 T to 5.5 T. Dielectric measurements were done using LCR meter with frequency range from 100 Hz to 1 MHz in a closed-cycle cryostat cooler allowing to cool the sample down to 10 K. Before measurements, Au electrodes were deposited in the opposite surfaces of the samples by dc-sputtering method.

3. Results and discussion

Table 1 gives the values of lattice constants, unit cell volume and weight fraction of the h-$LuMn_xO_{3\pm\delta}$ phase determined by Rietveld refinement of XRD spectra. The crystalline lattice of the $LuMn_xO_{3\pm\delta}$ phase in all samples fits the $P6_3cm$ space group as reported for stoichiometric h-$RMnO_3$ phases [2,6] (Fig.1a and b). Traces of Lu_2O_3 phase were detected in Lu-rich side (inset of Fig.1a), while on the Mn-rich the secondary phase was identified as Mn_3O_4 (inset of Fig.1b). The amount of secondary phase depends on the value of cation ratio x in the formulation of the samples. For the case of samples with Mn-excess $(x>1)$, the crystalline lattice of h-$LuMn_xO_{3\pm\delta}$ becomes saturated in Mn at the edge of the stability limit of the hexagonal manganite. At 1300 °C, any Mn added in excess to the saturation point will remain in the sample as Mn_3O_4 [23]. In the opposite direction, Lu excess remains as the Lu_2O_3 secondary phase once the solid solution limit for Lu in the h-$LuMn_xO_{3\pm\delta}$ is exceeded.

The Rietveld refinement could not yield a precise value for the fraction of the (minor) secondary phase. The values of the quality factor of the XRD Rietveld refinement, R_f-factor, in Table 1 generally suggest the occurrence of structural inhomogeneity inside the crystalline grains of the h-$LuMn_xO_{3\pm\delta}$ phase of the ceramic material. The lacking of homogeneity of the crystalline grains explains the difficulty found to establish the atomic positions of the ions in h-$LuMn_xO_{3\pm\delta}$ crystalline cell by Rietveld refinement. As shown in Table 1, the quality factor R_f for the sample of $x=1.08$ is poor, in agreement with the difficulty of detecting the hausmanite secondary phase by XRD in h-$RMnO_{3\pm\delta}$ compounds. The EDS analysis in SEM of polished cross sections of the samples confirmed the presence of the binary oxides as secondary phases in the form of isolated inclusions of 0.5–2 μm size of Lu_2O_3 in samples of low x and of 1–5 μm size of Mn_3O_4 in the samples of high values of x.

From the values of x of the sample composition, the weight fraction f of the main phase, h-$LuMn_xO_{3\pm\delta}$, determined by XRD, Table 1, the molecular weight of the secondary phases (the Lu_2O_3 or Mn_3O_4) assumed as pure phases, the value of the Mn/Lu ratio in the h-$LuMn_xO_{3\pm\delta}$ solid solution in contact with the corresponding residual phase was calculated as the root of the balance equation of x and it is given by x_r in Table 1. Based on the values of x_r found in the present study, the lower and upper boundaries of the domain of stability of the $LuMnO_3$ solid solution at 1300 °C are approximately set as $x_{Low}\approx 0.95$ and $x_{High}\approx 1.04$, respectively.

Albeit the scatter of the XRD Rietveld refinement results in Table 1, also shown in the plots of Fig. 2, the a-axis length and cell volume V_c of $LuMn_xO_{3\pm\delta}$ display a trend for decreasing of their values with increasing x. A similar decrease of axis lengths of the

Table 1
Results of the XRD Rietveld refinement, Neel magnetic ordering and Curie–Weiss temperture for hexagonal $LuMn_xO_{3\pm\delta}$ samples of composition in the range $0.92 \le x \le 1.12$.

x=Mn/Lu	0.92	0.96	0.98	1	1.02	1.04	1.08	1.12
a	6.0448	6.042	6.0409	6.0417	6.0427	6.0374	6.04006	6.0363
c	11.3681	11.3674	11.3682	11.3679	11.3709	11.3654	11.3671	11.3653
V_c, cell volume	359.74(2)	359.38(2)	359.25(2)	359.362(2)	359.57(2)	358.77(2)	359.14(1)	358.64(1)
Fraction (wt%)	97.28	99.65	99.35	100	98.25	97.75	98.81	97.42
R_I-Factor	1.98	4.03	2.64	4.08	3.31	2.2	2.79	2.14
Secondary phase	Lu_2O_3	Lu_2O_3	Lu_2O_3	–	Mn_3O_4	Mn_3O_4	Mn_3O_4	Mn_3O_4
Global χ^2	5.88	5.53	4.82	6.32	4.02	3.87	4.59	9
x_r (wt%)	0.955	0.965	0.989	1	n.a.	n.a.	1.035	1.021
T_N (K)	94.5	91.1	91.7	90.9	91.7	89.7	90	89.5
θ_{CW} (K)	−1126	−1145	−798	−671	−722	−645	−613	−673
$f(T_N/\theta_{CW})$	11.9	12.6	8.7	7.4	7.9	7.2	6.8	7.5

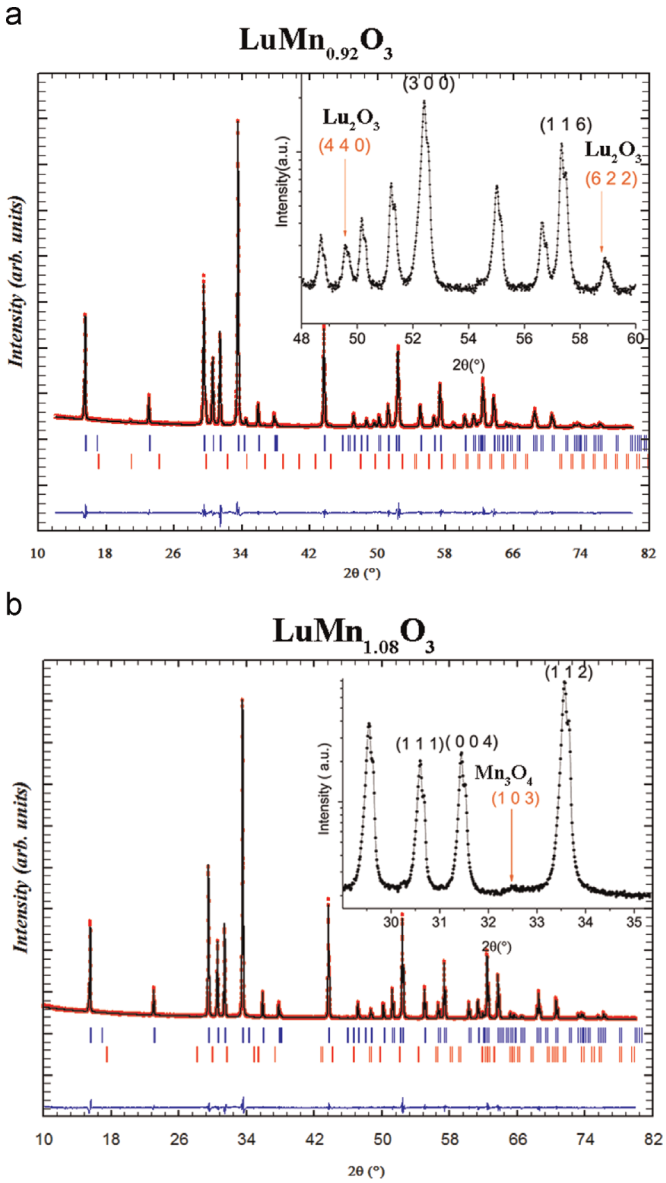

Fig. 1. XRD data and Rietveld Refinement of the data of the $LuMn_xO_{3\pm\delta}$ samples x= 0.92 (a) and x=1.08 (b) showing $P6_3cm$ space group of hexagonal $LuMnO_3$. Inset of (a) represents two peaks of Lu_2O_3 secondary phase of sample with x= 0.92 (2θ=49.58° and 58.9°) and the inset of (b) shows the peak of Mn_3O_4 secondary phase for sample with x=1.08 (2θ=32.5°).

crystalline cell had been reported for Y-rich side of the h-$YMn_xO_{3\pm\delta}$ solid solution [19]. As emphasized by the construction of Fig. 2 the changes of cell volume V_c are mostly correlated to the modification of a-axis with x_r. Within the limits of experimental

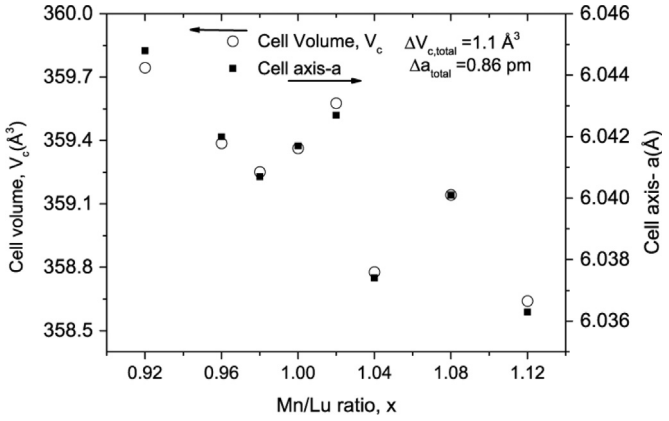

Fig. 2. Dependence of the crystalline lattice parameters, a-axis a and cell volume V_c of the $LuMn_xO_{3\pm\delta}$ phase on the ratio x=Mn/Lu.

error no correlation could be established between the c-axis length and the Mn/Lu ratio of $LuMn_xO_{3\pm\delta}$. For the Y-rich side of YMn_xO_3 solid solution, $0.91 \le x \le 1.00$, the following values of the dependences of total change of a-axis, c-axis length (data from Fig. 1a of Ref.[19]) and V_c on x were obtained, Δa=−0.6 pm, Δc=−0.9 pm, ΔV=−0.98 Å^3, respectively. The change of the crystalline lattice parameters of $LuMn_xO_{3\pm\delta}$ ($0.92 \le x \le 1.00$) from Table 1 are: Δa=−0.32 pm and ΔV=−0.4 Å^3, respectively. The change of a-lattice constant and V_c under the effect of Mn^{3+} vacancy in $LuMn_xO_{3\pm\delta}$ is almost twice the observed in $YMn_xO_{3\pm\delta}$ similar range of solid stability. The calculated change of the dependence of out-of-plane c-axis length on x of single phase MOCVD thin films deposited on (111) YSZ monocrystalline substrates (data of strain relaxed layer of the top of thin film c_2, from Fig. 3 of Ref. [12]) are Δc=−10.1 pm for $ErMn_xO_{3\pm\delta}$ ($0.89 \le x \le 1.00$) and Δc=−5.9 pm for $DyMn_xO_{3\pm\delta}$ ($0.93 \le x \le 1.00$), respectively. These values of Δc are a few times larger than the corresponding value of Δc of the $YMn_xO_{3\pm\delta}$ bulk samples above due to constraining of a-axis dimensions by the substrate during epitaxial film growing [12]. The same analysis of total change of Δc in a wider range of both Mn^{3+} or R^{3+} vacancies of $LuMn_xO_{3\pm\delta}$ ($0.92 \le x \le 1.12$), $ErMn_xO_{3\pm\delta}$ ($0.89 \le x \le 1.09$) and $DyMn_xO_{3\pm\delta}$ ($0.93 \le x \le 1.11$) results in 0.28 pm, 13.1 pm and 6.17 pm, respectively. From the values of Δa, Δc and ΔV_c one can conclude that in the case of thin films of the h-$RMn_xO_{3\pm\delta}$ phases the selection of most adequate substrates, YZS, STO or Al_2O_3 which may impose a pre-set value of Δa there is ample room to accommodate changes of c-axis hence for different degrees of coupling of the magnetic (in a–b plane) and ferroelectric (c-axis dominant) properties of the h-$RMn_xO_{3\pm\delta}$ solid solutions.

The values of T_N (from the minimum of the first derivative of the magnetic susceptibility) and θ_{CW} determined from the measurements of the magnetic susceptibility done by SQUID

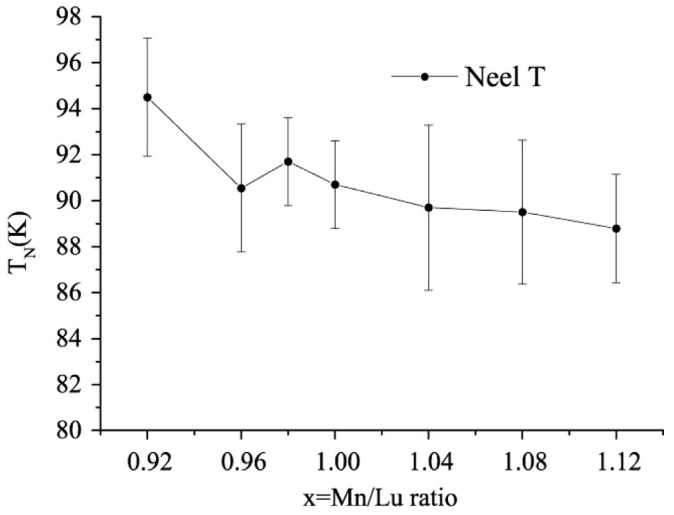

Fig. 3. Néel ordering transition temperature vs. x showing a decreasing trend as the x increases. The error bars are included to count the broadening of the first derivative peak (FWHM).

magnetometer, applied magnetic field of 100 Oe for all samples $LuMn_xO_{3\pm\delta}$ are given in Table 1. The temperature ranges of 150–300 K (or 150–350 K) were used for the linear fitting of χ^{-1} to T (after subtracting the magnetization originated from residual hausmannite phase, this contribution being calculated from XRD data and the magnetic properties of Mn_3O_4 [27]), for the given samples in Table 1. The corresponding estimated values of Curie–Weiss temperature, θ_{CW}, and frustration factor, $f_m = -\theta_{CW}/T_N$ are also given in Table 1. Fig. 3 indicates a decreasing trend of the T_N by adding more Mn to the compositions. The value of T_N for the stoichiometric sample is 90.9 K close to what is frequently reported in the literature [2,28]. The Curie–Weiss temperature of sample $x=1$ is –670 K. It is lower than the value for single crystal, –880K [2], and the one for ploycrystal, –760 K [29] being sintered at 1300 °C after 24 h, higher than the reported value of –520 K of the ploycrystals with final heating at 1400 °C for 48 h [28]. An increase of 4 K in Neel temperature from 68 K to 72 K was reported in bulk $YMn_xO_{3\pm\delta}$ samples Y-rich side, which adds to an almost equal increase of T_N from stoichiometry to $x_H \approx 1.08$ the upper limit of stability of the $YMn_xO_{3\pm\delta}$ solid solution [19,25]. The corresponding average rate of change of T_N with the Y/Mn ratio being $\Delta T_N/\Delta x = 60.5$ K mol^{-1} Mn. Such changes of T_N are coupled to the very large decrease of – 98 K in Curie–Weiss temperature from $x_L = 0.95$ to $x=1$ with an additional decrease of –212 K from $x=1$ to $x_H \approx 1.08$ [15,17], yielding the average rate of change $\Delta\theta_{CW}/\Delta x = -2409$ K mol^{-1} Mn. The analysis of the dependences of T_N and θ_{CW} on x of the data of the $LuMn_xO_{3\pm\delta}$ samples in Table 1 qualitatively indicates trends of opposite sign to those found in $YMn_xO_{3\pm\delta}$. The corresponding values for the average rate of change of these properties in the $LuMn_xO_{3\pm\delta}$ phase are $\Delta T_N/\Delta x_r \approx -47$ K mol^{-1} Mn and $\Delta\theta_{CW}/\Delta x_r \approx 7760$ K mol^{-1} Mn, respectively. No explanation for such coupled reversing of trends of T_N and θ_{CW} from $YMn_xO_{3\pm\delta}$ to the $LuMn_xO_{3\pm\delta}$ solid solutions was found to the present stage of the study.

Fig. 4a and b show the temperature dependence of the magnetic susceptibility with at magnetic field of 500 Oe for zero-field-cooled (ZFC) and field-cooled (FC) conditions of two samples with $x=0.92$ and $x=1.08$, respectively. Antiferromagnetic (AFM) ordering is seen for both compositions at values of Neel temperature T_N close to 90 K. Fitting of the reciprocal of the magnetic susceptibility, χ^{-1}, to the Curie–Weiss law, determined by SQUID magnetometer under ZFC condition, 100 Oe applied magnetic field, is presented in insets of Fig 4a and b.

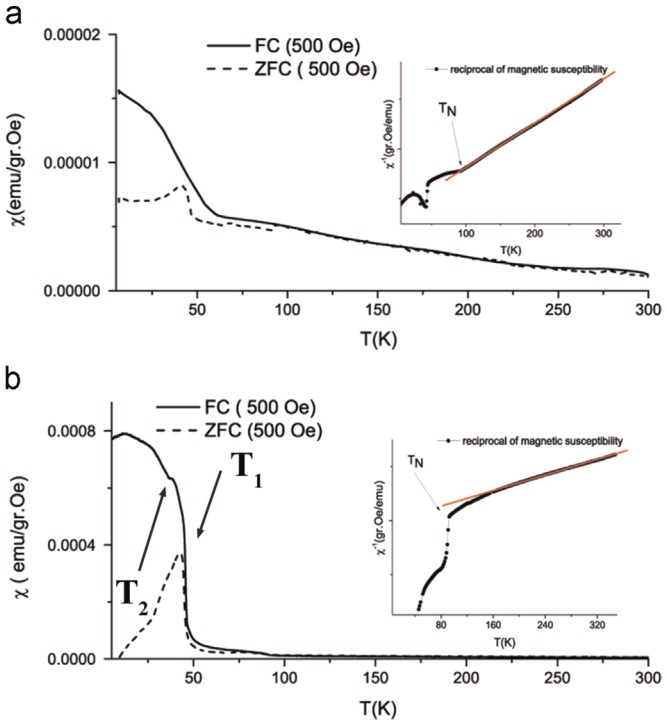

Fig. 4. Field-cooling (FC) and Zero-Field-Cooling (ZFC) magnetic susceptibility as a function of temperature at $H=500$ Oe measured in temperature range of 5–300 K on off-stoichiometric $LuMn_xO_{3\pm\delta}$ powders, (a) $x=0.92$ and (b) $x=1.08$. Inset of figures represents Curie–Weiss fitting to the reciprocal of FC magnetic susceptibility for two samples.

The increased Mn content of $LuMn_xO_{3\pm\delta}$ sample ($x=1.08$) in Fig. 4b resulted in neatly appearance of a magnetic cusp below T_N for ZFC magnetic susceptibility. Furthermore, by increasing the ratio x large differences of the magnetic susceptibility measured in ZFC and FC conditions appeared below T_N. Such irreversibility or spin-glass like behavior in ZFC/FC magnetic measurements was also observed in h-$RMnO_3$ [10,22,30–33]. The reciprocal of magnetic susceptibility, χ^{-1}, deviates from the linear dependency on temperature expected from Curie–Weiss law in the paramagnetic region approaching T_N. This behavior was previously reported by others for h-$LuMnO_3$ [29,34]. The deviation in measurements from Curie–Weiss law made it difficult to estimate the parameters of the Curie–Weiss law itself for the overall set off-stoichiometric samples of the present study.

The co-existence of frustrated AFM order and weak FM order below T_N observed in the temperature dependent magnetization of h-$RMnO_3$ was attributed to diverse causes such as the exchange coupling between AFM and FM orders [22,35], Mn spin reorientation and Dzyalloshinskii–Moriya interaction [10,33,36–38], double exchange interaction of Mn^{2+}/Mn^{4+} and Mn^{3+} ions [25] or local MnO_5 distortions [39]. By accounting for the secondary phases detected in off-stoichiometric samples, Table 1, in the Mn-rich side ($x>1$) the Mn_3O_4 phase will contribute to the magnetic signal below 43 K transition temperature [40] in proportion to the fraction of this phase present in the samples. That would not be case of samples in the Lu-rich side with $x \leq 1$ which still show a rising of magnetic susceptibility below T_N although of lower intensity (Fig. 4a), with no indication of Mn_3O_4 on XRD. The origin of the weak ferromagnetic component of χ had been tentatively explained as Dzyaloshinskii–Moriya exchange interaction, because of geometrically frustrated trimmers of the Mn ions in the basal plane [32,38,41]. The plot of χ^{-1} of Fig. 4b for the sample with $x=1.08$, shows two anomalies or transitions of the magnetic susceptibility below $T_N \approx 90$ K. The first transition at temperature T_1

in the range of 40 – 45 K is most likely correlated to the ferrimagnetism of the Mn_3O_4 phase. However the origin of the second transition corresponding to T_2, below 40 K is hardly known; it may originate from the spin reorientation of Mn^{3+} moment in $LuMnO_3$ [10,37]. The coexistence of different configurations of AFM order below T_N in $ScMnO_3$ was already observed by Second Harmonic Generation (SHG) spectroscopy having been assigned to inhomogeneity in the crystalline lattices [42]. In the Lu-excess side, the difference between ZFC and FC signals below T_N becomes weaker as the ratio x decreases. On the contrary, addition of excess Y ions to $YMn_{1+x}O_{3\pm\delta}$ ceramics ($x<1$) resulted in more pronounced irreversibility below T_N with a slight decreasing of T_N matched by an important increase in Curie–Weiss temperature, lower $|\theta_{CW}|$ [19]. The rising of θ_{CW} with minor changes of T_N implies a decrease of f_m, the frustration factor indicating that self-doping with *Y* weakens the geometrically frustrated magnetic interactions of Mn^{3+} ions in the basal plane of $YMnO_3$ ceramics [2].

In the self-doped $LuMn_xO_{3\pm\delta}$ ceramics of the current study the difficulty in accurately determining T_N is implicitly endorsed to structural fluctuation of Mn trimmers in basal plane due to vacancies, planar defects of the crystalline lattice and the resulting distortions of ion positions. The effect of vacancy promoted modifications in the arrangements of the Mn^{3+} ions is notable in the magnetic susceptibility data of two samples, $x=0.92$ and $x=1.12$, as they show the largest and lowest values of T_N in Table 1, respectively. The increasing of T_N for samples with $x<1$ such as $x=0.92$ sample in Fig. 3 cannot be explained on changes of the distance between two nearest-neighbor Mn^{3+} ions extracted from a-axis values, Table 1. As data clearly exhibit, when *x* decreases there is a growth of the a-axis and widening of the area of the crystalline cell face in the basal plane, therefore the AFM interaction of two neighboring Mn ions in basal plane would become weaker. The AFM interaction energy is a function of *J*, the superexchange integral mediated by the oxygen ion between the nearest neighbor Mn^{3+} ions in basal plane [43,44] . Based on the change of Mn^{3+} ion distances alone, such dependence of *J* would entail that AFM interaction among Mn moments would get stronger when the distance between two neighbor moments decreases as the value of in-plane exchange integral, *J*, rises with the reciprocal of the distance of two neighboring Mn^{3+} ions [45]. It would imply that the sample with larger Mn vacancy content ($x=0.92$) and wider a-axis would display weaker AFM interaction in basal plane and hence a lower value of T_N, if only atomic distances are considered in basal plane AFM interaction. Such interpretation seemingly holds for the self-doped $YMn_xO_{3\pm\delta}$ bulk samples [19,25]. In general, J also depends on ion bond angles and other factors. In the case of $LuMnO_{3\pm\delta}$ the MnO_5 bipyramids of materials with stoichiometric composition are slightly twisted, which was not the case of $YMnO_3$ [29,46]. However, given that the AFM interaction (*J*) of the Mn^{3+} ions depends also on the bond angles, the in-plane magnetic interaction of the Mn^{3+} ions becomes a function of trimmer distortion, too. The effect of Mn vacancy in $x<1$ side of $LuMn_xO_{3\pm\delta}$ and subsequent distortions induced in the lattice due to the vacant sites at the center of a fraction of the MnO_5 bipyramids has changed AFM scenario and resulted in higher T_N, lower θ_{CW} and hence more intense magnetic frustration, with larger f_m factors. Also, in the sample of $x=1.08$, the one with highest Lu vacancy concentration and hence with shortest a-axis, from the previous argument one would expect highest T_N but it is not so (Table 1). Again, here the Lu-vacancy in the building block of the unit cell of $LuMnO_3$ has probably induced distortions in the lattice and unit cell, generally weakening the AFM interaction

The field dependence of magnetization (*M–H*) was measured to characterize the weak ferromagnetism observed below T_N. Fig. 5a and b show the magnetic hysteresis loops of selected samples with $x=0.92$, $x=1.00$ and $x=1.08$, at 5 K and 80 K, respectively. Magnetic hysteresis extends up to Neel ordering temperature T_N, the ferromagnetic component being enhanced by increasing *x*. Hysteresis loops of the three samples at 5 K, Fig. 5a, indicate that the magnetic coercive field of samples with excess $x>1$ is larger than the magnetic coercivity of samples with $x\leq 1$. Fig. 6 shows the temperature dependency of remanent magnetization B_r and H_c at 80 K close to T_N for a selection of samples representing the system. Wide differences in the values of H_c and B_r become apparent for the samples with Mn excess, $x>1$, presenting much higher values of H_c and B_r. The contribution of hausmannite secondary phase in samples with $x>1$ (Table 1) results in wider hysteresis loops and in larger values of the coercive field and has to be accounted for in the analysis of the *M–H* cycles of these samples at 5 K [40,47]. The wide opening of *M–H* cycle at 5 K observed in Fig. 5a only for the sample $x=1.08$, with the large increase in the values of M_r and H_c coincides with the detection of Mn_3O_4 in the order of 1% in weight (Table 1) and maybe explained by the presence of such impurity. Previous studies of the detailed atomic structures of stoichiometric and off-stoichiometric h-$RMnO_3$ thin films revealed the presence of nano-inclusions or structural distortions in these materials [9,12,48–51]. The nano-inclusions and lattice distortions around these nano-regions will affect the tilting of bipyramids or arrangements of Mn^{3+} ions in basal plane. The increase of the coercive field H_c by the mounting Mn content in Fig. 5a and b points out the role of Mn-excess (or conversely the role of Lu vacancies) on modifying the magnetic properties of vacancy-doped

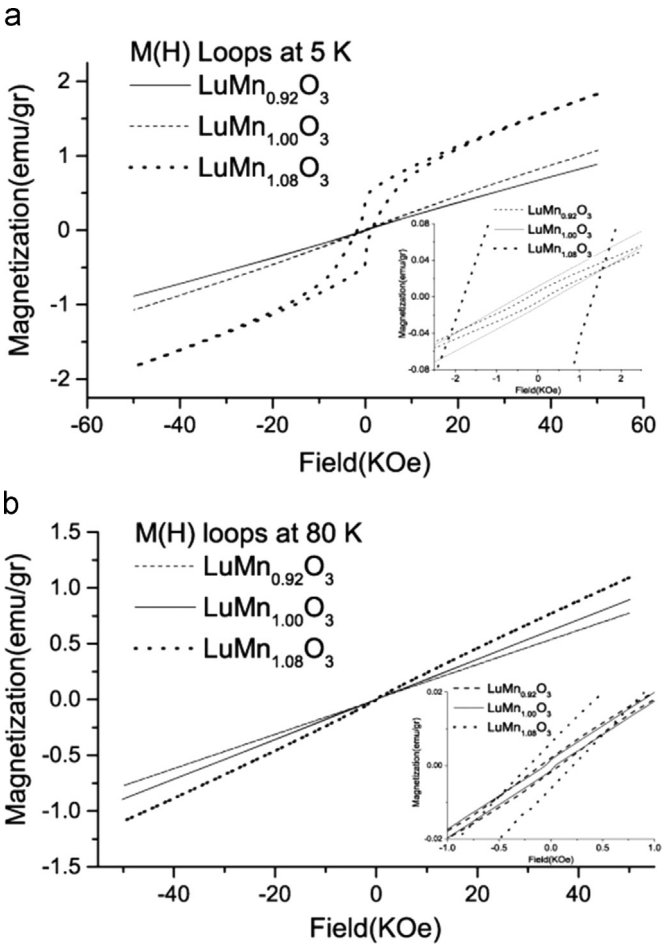

Fig. 5. Field dependent magnetization of selected $LuMn_xO_{3\pm\delta}$ samples ($x=0.92$, 1.00, and 1.08) at 5 K (a) and 80 K (b) in the range of 5.5 T to −5.5 T. Insets in (a) and (b) give enlarged views of the magnetic hysteresis at the origin of the axes.

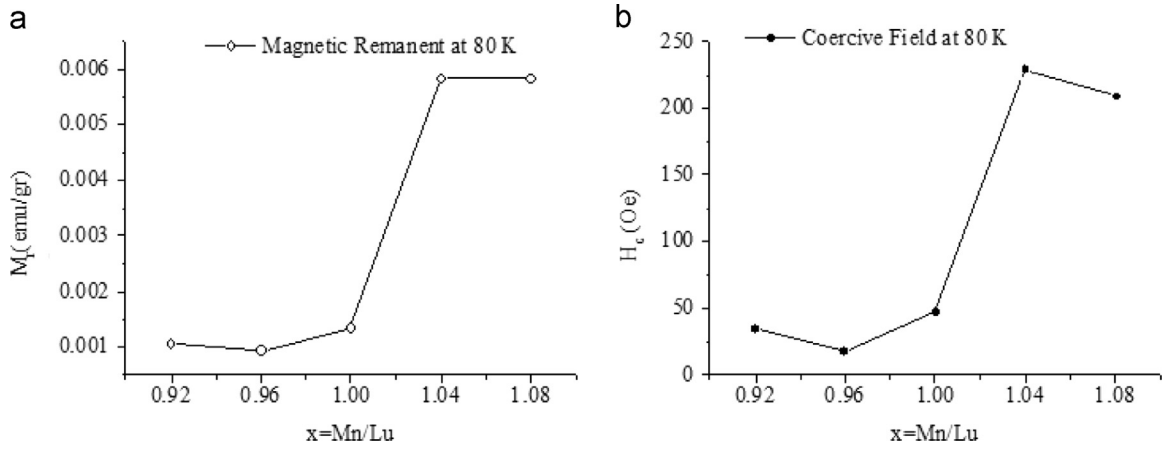

Fig. 6. Temperature dependence (a) of Remanent magnetization M_r and (b) the magnetic coercive field, H_c, of selected $LuMn_xO_{3\pm\delta}$ samples at 80 K. As shown, coercive field H_c and M_r increase as the Mn content (x) of samples increases.

samples [25,52].

AFM domain walls directly coupled by the magnetoelectric effect to the ferroelectric domain walls were reported in the ferroelectromagnetic h-$YMnO_3$ [53, 54]. The coupling of magnetization with the electrical polarization and its modifications in off-stoichiometric $LuMn_xO_{3\pm\delta}$ samples was also investigated. The dependence of the complex dielectric constant ε^* on temperature is assessed here both to clarify if the magnetic transitions described above also resulted in changes of dielectric polarization at the same temperatures [1,2] and in searching for changes of spin-phonon coupling and domain wall switching with off-stoichiometry of the $LuMn_xO_{3\pm\delta}$ samples [30,55,56]. Fig. 7 shows the temperature dependence of the real part of the dielectric constant $\varepsilon'(T)$ of samples with $x=1.00$, 1.04 and 1.08 measured at 1000 KHz. The T derivative of $\varepsilon'(T)$ of sample with $x=1.08$ in the frequency range 44.5 KHz to 1 MHz, is given in Fig. 8a. The temperature dependence of the imaginary dielectric constant $\varepsilon''(T)$ of sample $LuMn_{1.08}O_{3\pm\delta}$ determined in 11.2 KHz to 1 MHz frequency range is shown in Fig. 8.b. The main drop of ε'(T) of three $LuMn_xO_{3\pm\delta}$ samples at T_N coupled to the AFM ordering of the magnetic measurements is clearly apparent in Fig. 7. Besides the transition of ε'(T) with maximum of the derivative at $T1_{max}=89$ K ($\approx T_N$), Fig. 8a, the derivative of $\varepsilon'(T)$ of sample $LuMn_{1.08}O_{3\pm\delta}$ in Fig. 8a also indicates two other transitions: the one starting at 80 K which is broad and has the maximum of the derivative of $\varepsilon'(T)$ at $T2_{max}=69$ K and another at lower temperature with the maximum of the derivative of $\varepsilon'(T)$ at $T3_{max}=31$ K. Analogous anomaly of the dielectric constant coupled to a transition of the magnetic susceptibility was early observed in $YMnO_3$ polycrystalline samples prepared by the same solid state route of this study at a relative temperature similar to $T2_{max}/T_N$ ratio [34,57] . The transition of $\varepsilon'(T)$ at $T1_{max}\approx T_N$ closely coincides with the observed transitions in the magnetic susceptibility of the same sample in Fig. 4b. The two other transition temperatures $T2_{max}=69$ K and $T3_{max}=31$ K also exist on the second derivative of the magnetic susceptibility. The derivative of $\varepsilon'(T)$ of sample $LuMn_{1.08}O_{3\pm\delta}$ in the transitions at $T1_{max}\approx T_N$ and $T2_{max}$ for the different frequencies given in Fig. 8a exhibit inverse S-shape anomaly, not just when the sample entered AFM magnetic ordering region but also below T_N, which is seen as indication of coupling of the magnetic and dielectric order [57]. At all frequencies of the dielectric measurements the derivative of ε'(T) does not show any frequency dependency for the main peaks of two transitions at T_N and 69 K (Fig. 8.a); hence these transitions are correlated to athermal mechanisms of polarization. However the transition observed in ε'(T) at temperature $T3$max is neatly dependent on frequency, Fig. 8.a. The imaginary dielectric

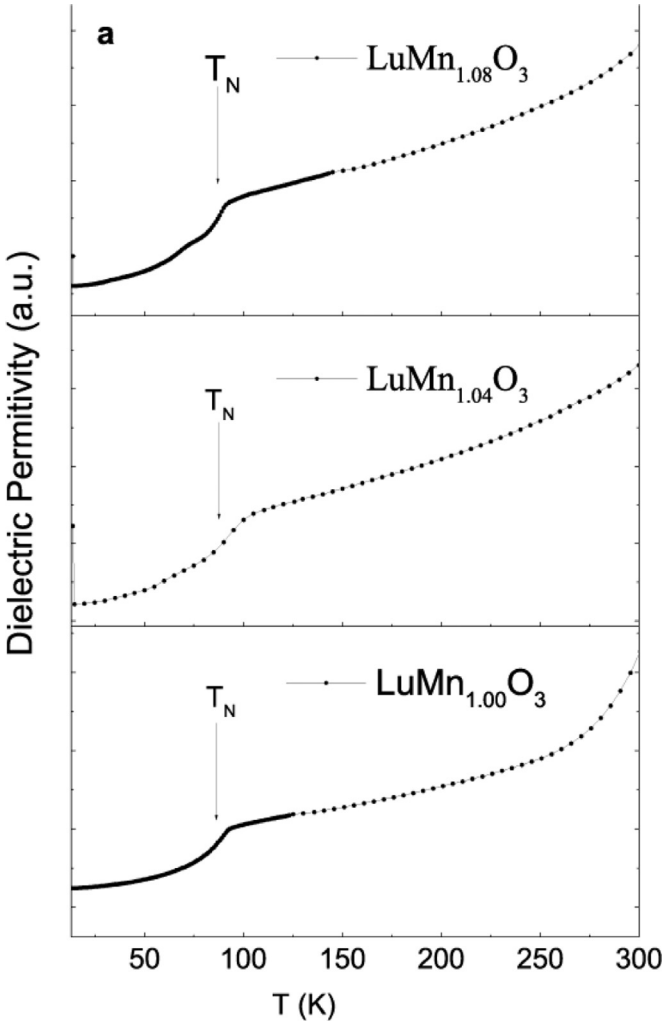

Fig. 7. Temperature dependence of real part of dielectric constant, $\varepsilon'(T)$, of selected $LuMn_xO_{3\pm\delta}$ samples with $x=1.00$, 1.04 and 1.08 at 1 MHz evidencing the drop of the dielectric constant ε'at T_N.

constant ε'' of all measured samples shows a near Debye relation. The dependency of $T3_{max}$ on frequency, shown in Fig. 8b for sample $LuMn_{1.08}O_{3\pm\delta}$, signals the thermally activated nature of the dielectric relaxation mechanism of such low temperature anomaly of the dielectric behavior. The shift of temperature of the peak with frequency in Fig. 8b can be traced from 18 K to 31 K

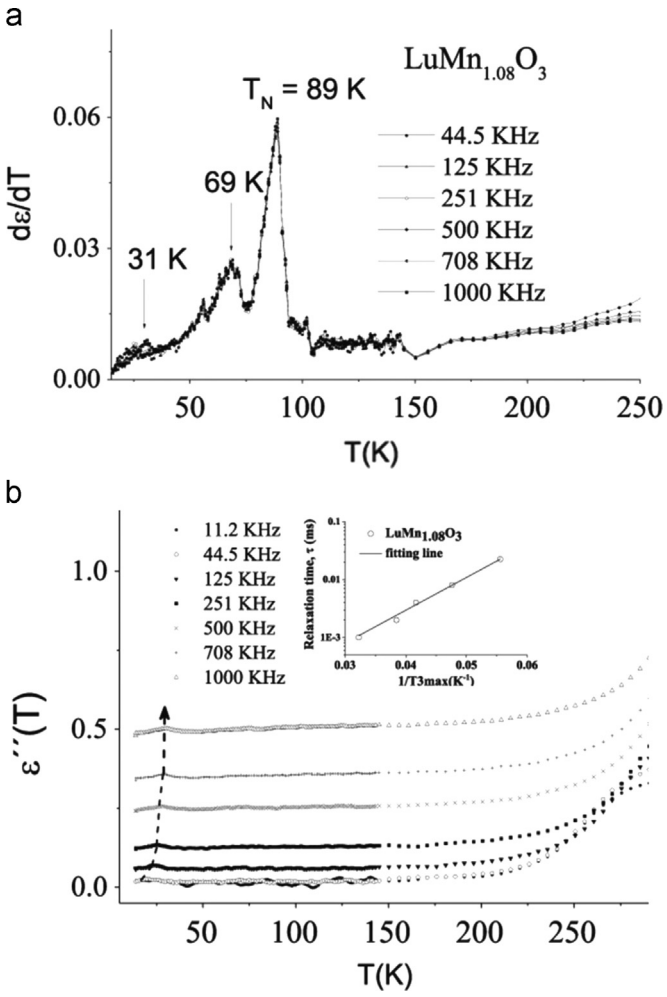

Fig. 8. (a) Temperature derivative of the dielectric constant ε' (T) at different frequencies for the sample $LuMn_{1.08}O_{3\pm\delta}$ indicating frequency independent peaks at 89 K and 69 K and a frequency dependent transition around 31 K. (b) Imaginary part of the dielectric constant $\varepsilon''(T)$ of same sample $LuMn_{1.08}O_{3\pm\delta}$ exhibiting the frequency dependence of the transition temperature of the transition observed around 31 K, inset with the Arrhenius plot of the relaxation time τ of the same anomaly of the dielectric constant.

corresponding to the frequencies above 40 KHz. For sample with $x=1.00$, this low temperature anomaly was observed only for frequencies above 100 KHz. The temperature range (18–31 K) of this anomaly of the complex dielectric constant, ε^*(T), of $LuMn_xO_{3\pm\delta}$ overlaps with the temperature of an analogous anomaly of real and imaginary components of $\varepsilon^*(T)$ centered at 23 K reported for the p-$Eu_{1-\xi}Lu_\xi MnO_3$ ($0 \le \xi \le 0.20$) solid solution, this phase retaining the perovskite crystalline structure for $\xi \le 0.30$ and converting to the hexagonal symmetry above this threshold [56,58]. The inset in Fig. 8b gives the Arrhenius plot of the relaxation time, $\tau=1/f$, of this anomaly, f being frequency of the dielectric measurement, a thermally activated mechanism where τ is given by $\tau(T)=\tau_0 \exp[U/k_BT]$, U is the activation energy, k_B the Boltzmann constant, and $T=T3_{max}$ is the temperature at the maximum of ε''. The increasing of the temperature of this maximum of $\varepsilon''$with frequency implies that faster switching of the dielectric dipoles demands higher thermal energy, the time dependent response of dielectric dipoles existing inside the ferroelectric domains delaying the response to the applied a.c. electric field. The line representing the fit to Arrhenius law in the inset of Fig. 8.b and yields the following values: $U=12$ meV and $\tau_0=12.5$ ns. These values of U and τ_0 reasonably match the corresponding values of the parameters of the polaron hopping mechanism of dielectric relaxation observed in the other ferroelectric materials, as determined for $Sr_{0.97}(Ti_{0.80}Fe_{0.20})O_{3-\delta}$ sintered samples, 75–150 K, with $U=60$ meV and $\tau_0=30$ ns [59] , as well as in the p-$Eu_{1-\xi}Lu_\xi MnO_3$ solid solution with $0.10 \le \xi \le 0.20$, 50–90 K, where $U=24$ meV and $25 \le \tau_0 \le 55$ ns [58]. The low temperature behavior of the $LuMn_xO_{3\pm\delta}$ samples ($x \ge 1$) and the values of τ_0 and U point to the presence of the polaron hopping [59,60] leading to a frequency dependent anomaly in dielectric constants, the effect becoming stronger as x increases.

Results of STEM analysis of structural domain walls in h-$RMnO_3$ and models based on ab-initio calculations corroborate the presence of anti-phase boundaries in ab-plane, the plane of strong AFM interactions of the Mn^{3+} ions [61,62]. It had also been proposed that the AFM as well as FE domain walls clamp to the structural domain walls and partial dislocations, their mutual interaction inducing the FM component along c-axis [62–64]. In addition, appearance of the other magnetic anomalies below T_N shows the effect of local inhomogeneity on the magnetic interaction which may be the direct result of structural changes inside the grains, in grain boundaries or sub-grain boundaries [34]. The dielectric polarization transitions at T_N and the one below T_N at $T2_{max}$ are coupled to AFM order as shown by the temperature dependence of dielectric permittivity, but not on frequency [34,57]. Therefore, the induced electrical polarization and the weak ferromagnetic component co-existing with AFM ordering are tentatively asserted as coupled to basal plane Mn–Mn AFM interactions coming from changes of Mn–O–Mn bond distances and angles as the a-axis and volume of unit cell are reduced by self-doping with Mn and a magnetic glass-like state becomes more neat.

4. Conclusion

The present findings highlight the role of structural inhomogeneity or lattice distortion on the magnetic interaction and dielectric behavior which may give rise to the new behavior of the multiferroic h-$RMnO_3$ materials beyond the more conventional description of multiferroism based on adjustments of R ionic radii but preserving the stoichiometry, expounded so far in the literature to the present for this class of materials. Introducing the off-stoichiometry in $RMnO_3$ ceramics as in the present study of h-$LuMn_xO_{3\pm\delta}$ bulk materials gives an additional tool to manipulate in a measurable amount the cell volume of the crystalline lattice mostly by the shrinkage of the a-axis and reduction of the area of the unit cell face in the a-b plane. Within the bounds of the stability limits of the h-$LuMn_xO_{3\pm\delta}$ phase, $0.95 \le x \le 1.04$ at 1300 °C in air, the observed modifications of the parameters of the Curie–Weiss law of the magnetic susceptibility in the paramagnetic state imposed by off-stoichiometry are large both below and above the point ($x=1$) of stoichiometric composition. Alteration of T_N, caused by off-stoichiometry of the h-$LuMn_xO_{3\pm\delta}$ phase is also seen. The observed change of the dielectric constant at T_N and the anomaly of the same property centered at 69 K are related to magneto-electric coupling in the hexagonal $LuMn_xO_{3\pm\delta}$ lattice. The frequency dependence of a low temperature anomaly of the dielectric constant that was traceable from 18 K to 31 K in stoichiometric and off-stoichiometric $LuMn_xO_{3\pm\delta}$ samples shows the mechanism of dielectric relaxation by polaron hoping. Resorting to the off-stoichiometry of the $RMn_xO_{3\pm\delta}$ ceramics as an additional tool to manipulate their physical properties, done with $LuMn_xO_{3\pm\delta}$ in the present study and reported for $YMn_xO_{3\pm\delta}$ in bibliography, may be generally applied on other rare-earth manganites of the same family.

The present results emphasize the needs of extending the studies on the atomic structures of h-$RMnO_3$ multiferroic

materials to the full stability range of the solid solutions, by the use of HRTEM by investigating the possible losing of the Mn oxidation state and unit cell distortion at the interfaces inside the crystalline grains of the solid solution. The results here describe also postulate that additional improvements in the homogeneity of the crystalline lattice of $LuMn_xO_{3\pm\delta}$ ceramics have to be gained by looking for better sintering and annealing conditions or by increasing the annealing time for the ions of the crystalline structure of the polycrystalline grains to find their ultimate positions of equilibrium.

Acknowledgments

The authors thank the financial support from the FCT Project PTDC/FIS/105416/2008 "MULTIFOX", CICECO-Aveiro Institute of Materials (Ref. FCT UID /CTM /50011/2013), financed by National Funds through the FCT/MEC and FCT fellowships SFRH/BPD/80663/2011 and SFRH/BPD/63942/2009.

References

[1] W. Eerenstein, N.D. Mathur, J.F. Scott, Multiferroic and magnetoelectric materials, Nature 442 (2006) 759–765, http://dx.doi.org/10.1038/nature05023.
[2] T. Katsufuji, M. Masaki, A. Machida, M. Moritomo, K. Kato, E. Nishibori, et al., Crystal structure and magnetic properties of hexagonal $RMnO_3$ (R=Y, Lu, and Sc) and the effect of doping, Phys. Rev. B 66 (2002) 134434, http://dx.doi.org/10.1103/PhysRevB.66.134434.
[3] S. Lee, A. Pirogov, J.H. Han, J.G. Park, A. Hoshikawa, T. Kamiyama, Direct observation of a coupling between spin, lattice and electric dipole moment in multiferroic $YMnO_3$, Phys. Rev. B. 71 (R) (2005) 180413, http://dx.doi.org/10.1103/PhysRevB.71.180413.
[4] X. Fabreges, S. Petit, I. Mirebeau, S. Pailhes, L. Pinsard, A. Forget, et al., Spin-Lattice Coupling, Frustration, and Magnetic Order in Multiferroic $RMnO_3$, Phys. Rev. Lett. 103 (2009) 067204, http://dx.doi.org/10.1103/PhysRevLett.103.067204.
[5] A. Oleaga, A. Salazar, D. Prabhakaran, J.G. Cheng, J.S. Zhou, Critical behavior of the paramagnetic to antiferromagnetic transition in orthorhombic and hexagonal phases of $RMnO_3$ (R=Sm, Tb, Dy, Ho, Er, Tm, Yb, Lu, Y), , Phys. Rev. B 85 (2012) 184425, http://dx.doi.org/10.1103/PhysRevB.85.184425.
[6] S. Lee, A. Pirogov, M. Kang, K.-H. Jang, M. Yonemura, T. Kamiyama, et al., Giant magneto-elastic coupling in multiferroic hexagonal manganites, Nature 451 (2008) 805–809, http://dx.doi.org/10.1038/nature06507.
[7] C. Zhang, X. Zhang, Y. Sun, S. Liu, Atomistic simulation of Y-site substitution in multiferroic h-$YMnO_3$, Phys. Rev. B 83 (2011) 054104, http://dx.doi.org/10.1103/PhysRevB.83.054104.
[8] N. Jiang, X. Zhang, Atomistic simulation of Mn-site substitution in multiferroic h- $YMnO_3$, J. Phys. Condens. Matter 24 (2012) 235402, http://dx.doi.org/10.1088/0953-8984/24/23/235402.
[9] J.S. White, M. Bator, Y. Hu, H. Luetkens, J. Stahn, S. Capelli, et al., Strain-induced ferromagnetism in antiferromagnetic $LuMnO_3$ thin films, Phys. Rev. Lett. 111 (2013) 037201, http://dx.doi.org/10.1103/PhysRevLett.111.037201.
[10] R. Das, A. Jaiswal, S. Adyanthaya, P. Poddar, Origin of magnetic anomalies below the neel temperature in nanocrystalline $LuMnO_3$, J. Phys. Chem. C. 114 (2010) 12104–12109, http://dx.doi.org/10.1021/jp103037r.
[11] T.-C. Han, J.-W. Chen, Y.-H. Liu, Y.-M. Hu, Grain size effect on magnetic and electric properties of $LuMnO_3$ nanocrystalline materials, J. Appl. Phys. (2013), http://dx.doi.org/10.1063/1.4794977 17B507.
[12] I. Gelard, N. Jehanathan, H. Roussel, S. Gariglio, O.I. Lebedev, G. Van Tendeloo, et al., Off-stoichiometry effects on the crystalline and defect structure of hexagonal manganite $REMnO_3$ films (RE=Y, Er, Dy), Chem. Mater. 23 (2011) 1232–1238, http://dx.doi.org/10.1021/cm1029358.
[13] S.-H. Liu, J.-C.-A. Huang, X. Qi, W.-J. Lin, Y.-J. Siao, C.-R. Lin, et al., Structural transformation and charge transfer induced ferroelectricity and magnetism in annealed $YMnO_3$, AIP Adv. 1 (2011) 032173, http://dx.doi.org/10.1063/1.3647519.
[14] M. Palcut, K. Wiik, T. Grande, Cation self-diffusion and nonstoichiometry of lanthanum manganite studied by diffusion couple measurements, J. Phys. Chem. C 111 (2007) 813–822, http://dx.doi.org/10.1021/jp0642746.
[15] S. Chandra, A. Biswas, S. Datta, B. Ghosh, V. Siruguri, A.K. Raychaudhuri, et al., Evidence of a canted magnetic state in self-doped $LaMnO_{3+\delta}$ (δ=0.04): a magnetocaloric study, J. Phys.-Condens. Matter (2012), http://dx.doi.org/10.1088/0953-8984/24/36/366004.
[16] B. Fisher, J. Genossar, L. Patlagan, G.M. Reisner, Nonlinear conductivity of electronic origin in self-doped $LaMnO_{3+\delta}$, Appl. Phys. Lett. (2009), http://dx.doi.org/10.1063/1.3242008 132501–3.
[17] A.M.L. Lopes, J.P. Araujo, J.J. Ramasco, V.S. Amaral, R. Suryanarayanan, J. G. Correia, Percolative transition on ferromagnetic insulator manganites: uncorrelated to correlated polaron clusters, Phys. Rev. B. 73 (2006) 100408(R), http://dx.doi.org/10.1103/PhysRevB.73.100408.
[18] A. Lopes, J. Araújo, V. Amaral, J. Correia, Y. Tomioka, Y. Tokura, New phase transition in the $Pr_{1-x}Ca_xMnO_3$ system: evidence for electrical polarization in charge ordered manganites, Phys. Rev. Lett. 100 (2008) 155702, http://dx.doi.org/10.1103/PhysRevLett.100.155702.
[19] L. Jeuvrey, O. Pena, A. Moure, C. Moure, Synthesis and magnetic properties of hexagonal $Y(Mn,Cu)O_3$ multiferroic materials, J. Magn. Magn. Mater. 324 (2012) 717–722, http://dx.doi.org/10.1016/j.jmmm.2011.09.002.
[20] V.F. Balakirev, A.M. Yankin, O.M. Fedorova, L.B. Vedmid, Y.V. Golikov, Phase diagrams for systems formed by manganese and rare earth metal oxides, Russ. J. Inorg. Chem. 55 (2010) 1774–1778, http://dx.doi.org/10.1134/s0036023610110148.
[21] W.R. Chen, F.C. Zhang, J. Miao, B. Xu, L.X. Cao, X.G. Qiu, et al., Magnetic properties of the self-doped yttrium manganites $YMn_{1+x}O_3$, J. Phys.-Condens. Matter (2005), http://dx.doi.org/10.1088/0953-8984/17/50/0208029–8036 (2005), http://dx.doi.org/10.1088/0953-8984/17/50/020.
[22] M. Kumar, R.J. Choudhary, D.M. Phase, Metastable magnetic state and exchange bias training effect in Mn-rich $YMnO_3$ thin films, J. Phys. D. Appl. Phys. 48 (2015) 125003, http://dx.doi.org/10.1088/0022-3727/48/12/125003.
[23] O.M. Fedorova, Y.V. Golikov, Homogeneity ranges for yttrium and holmium manganites $Ln_{(2-x)}Mn_{(x)}O_{3\pm\delta}$ (Ln=Y, Ho) in air, Russ. J. Appl. Chem. 84 (2011) 512–514, http://dx.doi.org/10.1134/s1070427211030323.
[24] O.M. Fedorova, V.F. Balakirev, Y.V. Golikov, Homogeneity regions of yttrium and ytterbium manganites in air, Russ. J. Inorg. Chem. 56 (2011) 173–175, http://dx.doi.org/10.1134/s0036023611020070.
[25] W.R. Chen, F.C. Zhang, J. Miao, B. Xu, X.L. Dong, L.X. Cao, et al., Re-entrant spin glass behavior in Mn-rich $YMnO_3$, Appl. Phys. Lett. 87 (2005) 042508, http://dx.doi.org/10.1063/1.1991980.
[26] J. Rodriguez carvajal, Recenet advances in magnetic- structure determination by neutron powder diffraction, Phys. B. (1993), http://dx.doi.org/10.1016/0921-4526(93)90108-i55–69 (1993), http://dx.doi.org/10.1016/0921-4526(93)90108-i.
[27] G. Srinivasan, M. Seehra, Magnetic properties of Mn_3O_4 and a solution of the canted-spin problem, Phys. Rev. B 28 (1983) 1–7, http://dx.doi.org/10.1103/PhysRevB.28.1.
[28] D.G. Tomuta, S. Ramakrishnan, G.J. Nieuwenhuys, J.A. Mydosh, The magnetic susceptibility, specific heat and dielectric constant of hexagonal $YMnO_3$, $LuMnO_3$ and $ScMnO_3$, J. Phys. Condens. Matter 13 (2001) 4543–4552, http://dx.doi.org/10.1088/0953-8984/13/20/315.
[29] J.G. Park, S. Lee, M. Kang, K.-H. Jang, C. Lee, S.V. Streltsov, et al., Doping dependence of spin-lattice coupling and two-dimensional ordering in multiferroic hexagonal $Y_{1-x}Lu_xMnO_3$ ($0\le x\le 1$), Phys. Rev. B 82 (2010) 054428, http://dx.doi.org/10.1103/PhysRevB.82.054428.
[30] A. Ghosh, J.R. Sahu, S.V. Bhat, C.N.R. Rao, A Raman study of multiferroic $LuMnO_3$, Solid State Sci. 11 (2009) 1639–1642, http://dx.doi.org/10.1016/j.solidstatesciences.2009.06.002.
[31] K. Yoshii, H. Abe, Magnetic properties of $LnMnO_3$ (Ln=Ho, Er,Tm,Yb, and Lu), J. Solid State Chem. 165 (2002) 131–135, http://dx.doi.org/10.1006/jssc.2001.9514.
[32] Y.J. Yoo, Y.P. Lee, J.S. Park, J.H. Kang, J. Kim, B.W. Lee, et al., Spin-glass behavior of Cr-doped $YMnO_3$ compounds, J. Appl. Phys. 112 (2012) 013903, http://dx.doi.org/10.1063/1.4731631.
[33] A. Munoz, J.A. Alonso, M.J. Martinez-Lope, M.T. Casais, J.L. Martinez, M. T. Fernandez-Diaz, et al., Magnetic structure of hexagonal $RMnO_3$ (R=Y, Sc): Thermal evolution from neutron powder diffraction data, Phys. Rev. B 62 (2000) 9498–9510, http://dx.doi.org/10.1103/PhysRevB.62.9498.
[34] T. Katsufuji, S. Mori, M. Masaki, Y. Moritomo, N. Yamamoto, H. Takagi, Dielectric and magnetic anomalies and spin frustration in hexagonal $RMnO_3$ (R=Y, Yb, and Lu), Phys. Rev. B 64 (2001) 104419, http://dx.doi.org/10.1103/PhysRevB.64.104419.
[35] C. Zhang, J. Su, X. Wang, F. Huang, J. Zhang, Y. Liu, et al., Study on magnetic and dielectric properties of $YMnO_3$ ceramics, J. Alloys Compd. 509 (2011) 7738–7741, http://dx.doi.org/10.1016/j.jallcom.2011.04.128.
[36] P.A. Sharma, J.S. Ahn, N. Hur, S. Park, S.B. Kim, S. Lee, et al., Thermal conductivity of geometrically frustrated, ferroelectric $YMnO_3$: extraordinary spin–phonon interactions, Phys. Rev. Lett. (2004), http://dx.doi.org/10.1103/PhysRevLett.93.177202 177202–1.
[37] M. Bieringer, J.E. Greedan, Magnetic structure and spin reorientation transition in $ScMnO_3$, J. Solid State Chem. 143 (1999) 132–139, http://dx.doi.org/10.1006/jssc.1998.8127.
[38] K. Singh, M.-B. Lepetit, C. Simon, N. Bellido, S. Pailhes, J. Varignon, et al., Analysis of the multiferroicity in the hexagonal manganite $YMnO_3$, J. Phys.-Conden. Matter 25 (2013) 416002, http://dx.doi.org/10.1088/0953-8984/25/41/416002.
[39] S. Yano, D. Louca, S. Chi, M. Matsuda, Intertwining of frustration with magneto-elastic coupling in the multiferroic $LuMnO_3$, J. Phys. Soc. Jpn. 024601 (2013) 2–5, http://dx.doi.org/10.7566/JPSJ.83.024601 (accessed 14.01.15) http://dx.doi.org/10.7566/JPSJ.83.024601.
[40] R. Tackett, G. Lawes, B.C. Melot, M. Grossman, E.S. Toberer, R. Seshadri, Magnetodielectric coupling in Mn_3O_4, Phys. Rev. B 76 (2007) 024409, http://dx.doi.org/10.1103/PhysRevB.76.024409.
[41] S. Pailhes, X. Fabreges, L.P. Regnault, L. Pinsard-Godart, I. Mirebeau, F. Moussa, et al., Hybrid Goldstone modes in multiferroic $YMnO_3$ studied by polarized inelastic neutron scattering, Phys. Rev. B 79 (2009) 134409, http://dx.doi.org/

10.1103/PhysRevB.79.134409.
[42] M. Fiebig, D. Frohlich, K. Kohn, S. Leute, T. Lottermoser, V.V. Pavlov, et al., Determination of the magnetic symmetry of hexagonal manganites by second harmonic generation, Phys. Rev. Lett. 84 (2000) 5620–5623, http://dx.doi.org/10.1103/PhysRevLett.84.5620.
[43] J.G. Lin, Y.S. Chen, T.C. Han, Correlation of magnetic ordering and electric polarization in multiferroic $LuMn_{1-x}Fe_xO_3$ ($0 \le x \le 0.2$), J. Appl. Phys. 107 (2010) 09D902, http://dx.doi.org/10.1063/1.3360355.
[44] K. Charles, Introduction to Solid State Physics, 7th edition, John Wiley and Sons, Inc., New York, 1995.
[45] D. Bloch, 10/3 law for volume dependance of superexchange, J. Phys. Chem. Solids. 27 (1966) 881, http://dx.doi.org/10.1016/0022-3697(66)90262-9.
[46] T.-C. Han, W.-L. Hsu, W.-D. Lee, Grain size-dependent magnetic and electric properties in nanosized $YMnO_3$ multiferroic ceramics, Nanoscale Res. Lett. 6 (2011) 201, http://dx.doi.org/10.1186/1556-276x-6-201.
[47] T. Suzuki, T. Katsufuji, Magnetodielectric properties of spin-orbital coupled system Mn_3O_4, Phys. Rev. B. 77 (R) (2008) 220402, http://dx.doi.org/10.1103/PhysRevB.77.220402.
[48] N. Jehanathan, O. Lebedev, I. Gelard, C. Dubourdieu, G. Van Tendeloo, Structure and defect characterization of multiferroic $ReMnO_3$ films and multilayers by TEM, Nanotechnology. (2010), http://dx.doi.org/10.1088/0957-4484/21/7/075705 075705–11.
[49] T. Kordel, C. Wehrenfennig, D. Meier, T. Lottermoser, M. Fiebig, I. Gelard, et al., Nanodomains in multiferroic hexagonal $RMnO_3$ films (R=Y, Dy, Ho, Er), Phys. Rev. B (2009), http://dx.doi.org/10.1103/PhysRevB.80.045409 045409–8.
[50] T. Choi, Y. Horibe, H.T. Yi, Y.J. Choi, W. Wu, S.-W.W. Cheong, Insulating interlocked ferroelectric and structural antiphase domain walls in multiferroic $YMnO_3$, Nat. Mater. 9 (2010) 253–258, http://dx.doi.org/10.1038/nmat2632.
[51] I. Iliescu, M. Boudard, L. Rapenne, O. Chaix-Pluchery, H. Roussel, H. Roussel Laboratoire, MOCVD selective growth of orthorhombic or hexagonal $YMnO_3$ phase on Si(100) substrate, Appl. Surf. Sci. 306 (2014) 27–32, http://dx.doi.org/10.1016/j.apsusc.2014.01.090.
[52] C.R. Sankar, P.A. Joy, Magnetic properties of the self-doped lanthanum manganites $La_{1-x}MnO_3$, Phys. Rev. B 72 (2005) 024405–024410, http://dx.doi.org/10.1103/PhysRevB.72.024405.
[53] M. Fiebig, T. Lottermoser, D. Frohlich, A.V. Goltsev, R.V. Pisarev, Observation of coupled magnetic and electric domains, Nature 419 (2002) 818–820, http://dx.doi.org/10.1038/nature01077.
[54] A.V. Goltsev, R.V. Pisarev, T. Lottermoser, M. Fiebig, Structure and interaction of antiferromagnetic domain walls in hexagonal $YMnO_3$, Phys. Rev. Lett (2003), http://dx.doi.org/10.1103/PhysRevLett.90.177204 177204–1.
[55] N. Hur, I.K. Jeong, M.F. Hundley, S.B. Kim, S.W. Cheong, Giant magnetoelectric effect in multiferroic $HoMnO_3$ with a high ferroelectric transition temperature, Phys. Rev. B 79 (2009) 134120–134124, http://dx.doi.org/10.1103/PhysRevB.79.134120.
[56] D.A. Mota, Y. Romaguera Barcelay, P.B. Tavares, M.R. Chaves, A. Almeida, J. Oliveira, et al., Competing exchanges and spin-phonon coupling in $Eu_{1-x}R_xMnO_3$ (R=Y, Lu), J. Phys. Condens. Matter 25 (2013) 235602 (7 pp.).
[57] Z.J. Huang, Y. Cao, Y.Y. Sun, Y.Y. Xue, C.W. Chu, Coupling between the ferroelectric and antiferromagnetic orders in $YMnO_3$, Phys. Rev. B 56 (1997) 2623–2626, http://dx.doi.org/10.1103/PhysRevB.56.2623.
[58] J. Oliveira, J.A. Moreira, A. Almeida, M.R. Chaves, J.M.M. da Silva, J.B. Oliveira, et al., Phase diagram of the orthorhombic, lightly lutetium doped $EuMnO_3$ magnetoelectric system, Phys. Rev. B 84 (2011) 94414, http://dx.doi.org/10.1103/PhysRevB.84.094414.
[59] C. Ang, J.R. Jurado, Z. Yu, M.T. Colomer, J.R. Frade, J.L. Baptista, Variable-range-hopping conduction and dielectric relaxation in disordered $Sr_{0.97}(Ti_{1-x}Fe_x)O_{3-\delta}$, Phys. Rev. B 57 (1998) 11858–11861, http://dx.doi.org/10.1103/PhysRevB.57.11858.
[60] S. Komine, E. Iguchi, Dielectric properties in $LaFe_{0.5}Ga_{0.5}O_3$, J. Phys. Chem. Solids 68 (2007) 1504–1507, http://dx.doi.org/10.1016/j.jpcs.2007.03.024.
[61] Y. Kumagai, N.A. Spaldin, Structural domain walls in polar hexagonal manganites, Nat. Commun. 4 (2013) 1, http://dx.doi.org/10.1038/ncomms2545.
[62] Q.-H. Zhang, G.-T. Tan, L. Gu, Y. Yao, C.-Q. Jin, Y.-G. Wang, et al., Topology breaking of the vortex in multiferroic $Y_{0.67}Lu_{0.33}MnO_3$, Appl. Phys. Lett. 105 (2014) 012902, http://dx.doi.org/10.1063/1.4887057.
[63] S. Artyukhin, K.T. Delaney, N. a Spaldin, M. Mostovoy, Landau theory of topological defects in multiferroic hexagonal manganites, Nat. Mater. 13 (2014) 42–49, http://dx.doi.org/10.1038/nmat3786.
[64] H. Das, A.L. Wysocki, Y. Geng, W. Wu, C.J. Fennie, Bulk magnetoelectricity in the hexagonal manganites and ferrites, Nat. Commun. 5 (2014) 1–11, http://dx.doi.org/10.1038/ncomms3998.